Tungsten (2019) 1:187–197
https://doi.org/10.1007/s42864-019-00022-9

Tungsten
www.springer.com/42864

REVIEW PAPER

The thermal stability of dispersion-strengthened tungsten as plasma-facing materials: a short review

Tao Zhang[1] · Zhuoming Xie[2] · Junfeng Yang[2] · Ting Hao[2] · Changsong Liu[2]

Received: 11 June 2019 / Revised: 1 August 2019 / Accepted: 2 August 2019 / Published online: 11 September 2019

Abstract
One key challenge for the development of fusion energy is plasma-facing materials. Tungsten-based materials are promising candidates for plasma-facing components (PFCs) in the magnetic confinement nuclear fusion reactors because of their high melt temperature, high-thermal conductivity, high-thermal load resistance, low tritium retention, and low sputtering yield. In fusion reactors, PFCs are exposed to high-thermal flux, because there are some transient events such as plasma disruptions, edge-localized modes, and vertical displacement events (VDEs). Especially, in VDEs, a heat flux of 10–100 MW m^{-2} with duration of milliseconds-to-several seconds can induce recrystallization and then change the microstructure of tungsten-based plasma-facing materials, leading to instability of microstructures. Then, a significant degradation of material properties is caused such as a reduction of mechanical strength and fracture toughness, a rise in the ductile-to-brittle-transition temperature well, and decrease of irradiation/high-thermal load resistance. Therefore, many efforts were devoted to improve the thermal stability of tungsten-based materials as high as possible, such as oxide dispersion strengthening, carbide dispersion strengthening, and K bubbles dispersion strengthening. Here, the thermal stabilities of various dispersion-strengthened tungsten materials are reviewed by evaluating their recrystallization temperature and the corresponding hardness evolutions. In addition, the possible development trends are proposed.

Keywords Tungsten · Plasma-facing materials · Thermal stability · Dispersion strengthening

1 Introduction

Tungsten is a promising candidate for plasma-facing materials (PFMs) in future fusion reactors because of its excellent thermal diffusivity, low sputtering yield, high stability, and high hardness/strength, which all together can result in a long lifetime of plasma-facing components (PFCs) [1–5]. In spite of these advantages, the challenge of tungsten materials as PFMs is also noticeable, because PFMs are directly exposed to extreme conditions in the fusion plasma, such as high-energy neutron irradiation, high-thermal flux (0.1–20 MW m^{-2}) [5–7], sputtering erosion induced by high flux plasma with low energy, blistering, and exfoliation, transient events such as plasma disruptions, edge-localized modes (ELMs), and vertical displacement events (VDEs). During these transient events, it is expected that PFCs are exposed to high-thermal shocks. Especially, in VDEs, a heat flux of 10–100 MW m^{-2} with duration of milliseconds-to-several seconds is predicted [8–12]. The transient high energy acting on W materials leads to simultaneously high stress and high surface temperatures, destroying the original microstructure of tungsten materials by recrystallization and surface melting. The grain growth induced by recrystallizaiton can lead to the resegregation of impurities such as O, N, and P on the grain boundaries (GBs), decreasing the cohesion of GBs and inducing GB embrittlement. More importantly, recrystallization in W materials will result in producing new GBs with disordered orientations [13]. These unstable high-energy state random GBs are favorable sites for crack formation and thus easy to fracture as referred as recrystallization embrittlement which causes a significant degradation of properties such as the loss of mechanical strength,

✉ Tao Zhang
zhangtao@gzhu.edu.cn

✉ Zhuoming Xie
zmxie@issp.ac.cn

[1] School of Physics and Electronic Engineering, GuangZhou University, Guangzhou 510006, China

[2] Institute of Solid State Physics, Chinese Academy of Sciences, Hefei 230031, China

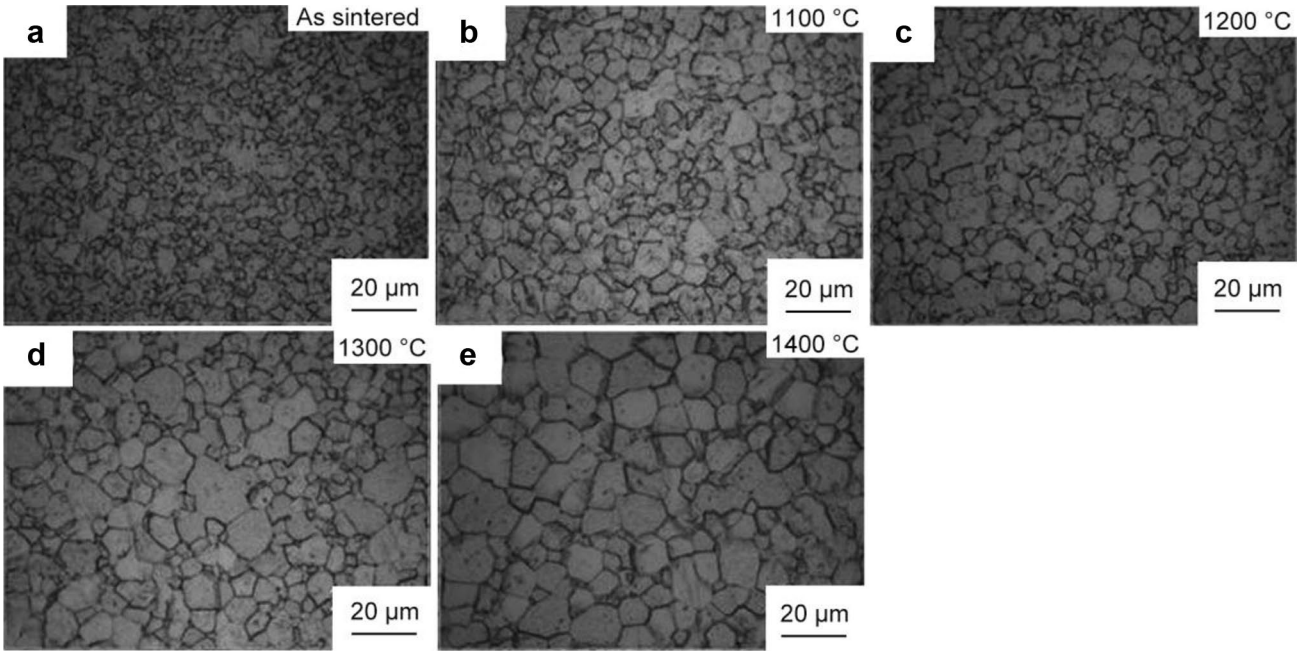

Fig. 1 Optical micrographs of as SPSed and annealed pure W. Reproduced with permission from Ref. [34]. Copyright 2015 Elsevier

reduction of fracture toughness, rise of the ductile-to-brittle-transition temperature (DBTT), and weakness of irradiation/thermal load resistances [14–16]. Therefore, increasing the thermal stability is desirable for PFMs.

The thermal stability can be characterized by recrystallization temperature (RCT), at which the new grains begin to form and grow up after annealing. It is well known that dispersion strengthening is an effective method to improve the performance of tungsten, especially to raise RCT. The nanoparticles pin and hinder the migration of GBs and dislocations in tungsten, which enhance the strength and creep resistance as well as the thermal stability by raising RCT. In addition, the dispersion of nanoscale particles produces a great number of phase interfaces that could act as sinks for irradiation-induced point defects, and thus could improve the irradiation resistance. For examples, oxides (e.g., La_2O_3 and Y_2O_3) or carbides (e.g., TiC, ZrC, TaC, and HfC) or nanosized K bubbles were introduced into W matrix to form the oxide or carbide dispersion-strengthened (ODS or CDS) and K-doped W materials [6, 17–29]. And recently, a series of ODS-W or CDS-W materials with enhanced thermal stabilities were developed. For example, the strength, RCT, and thermal shock resistances of W–La_2O_3 and W–Y_2O_3 were enhanced compared with pure W [6, 17, 24, 27, 30]. The carbides such as SiC, TiC, ZrC, TaC, and HfC, having higher melting temperatures and better compatibility with tungsten, were used to develop CDS-W which may lead to excellent thermal stability [20–23, 25, 28, 31–33]. To give a comprehensive insight, in this paper, the thermal stabilities of these newly developed ODS-W, CDS-W, and K-doped W materials are reviewed.

2 Thermal stability of pure W, K-doped, and oxide dispersion-strengthened W alloys

Xie et al. [34] prepared pure W by spark plasma sintering (SPS) and investigated the recrystallization behaviour by annealing at different temperatures for 1 h. Figure 1 shows the metallographic images of SPSed and annealed W at different temperatures. It can be seen that the grain size of SPSed W is ~ 4.4 μm, and after annealing at 1100 °C for 1 h, the grain size grows up to 5.3 μm. In this sense, the RCT should be between 1000 and 1100 °C. To further investigate the recrystallization behaviour of tungsten for applications of engineering, Deng et al. [19] fabricated a pure W plate by pressure-less sintering in hydrogen and hot rolling, because rolling deformation can eliminate the pores, densify materials, and further improve the mechanical properties of W [21, 35]. The metallographic images of rolled pure W before and after annealing are presented in Fig. 2 [19]. When annealing below 1300 °C, the grain size keeps almost constant, but when annealing above 1300 °C, the grains grow significantly. This RCT is almost the same as that reported in Refs. [36, 37], as shown in Fig. 3. It is noticeable that the RCTs of hot-rolled pure W are raised to temperature between 1200 and 1300 °C, which is much higher than that of SPSed pure W. The possible reason is that the grain size of SPSed

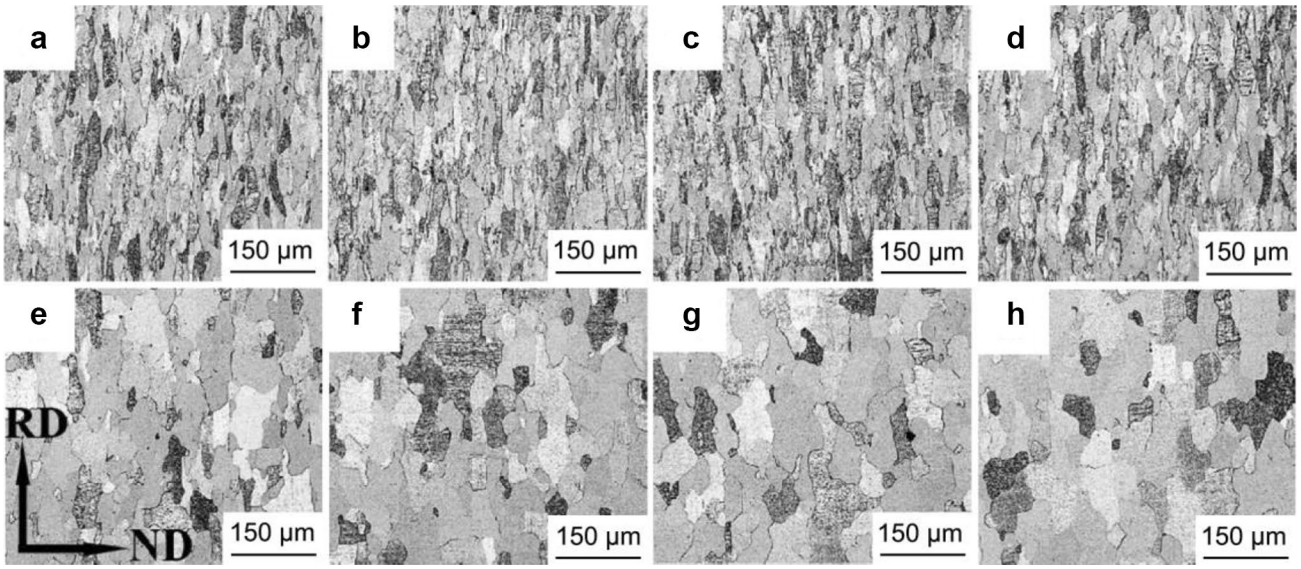

Fig. 2 Optical micrographs of the **a** as-rolled pure W, **b**–**h** pure W annealed at 1000 °C, 1100 °C, 1200 °C, 1300 °C, 1400 °C, 1500 °C, and 1600 °C, respectively. Reproduced with permission from Ref. [19]. Copyright 2018 Elsevier

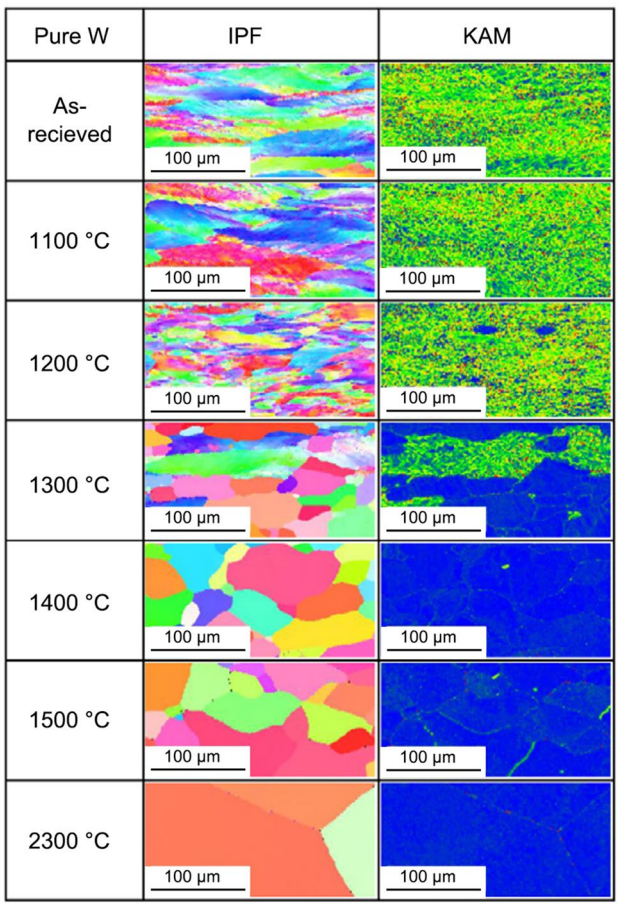

Fig. 3 Changes of the grain structure in pure W by isochronous annealing for 1 h. Here, IPF is the inverse pole figure, and KPM is the kernel average misorientation, respectively. Reproduced with permission from Ref. [36]. Copyright 2018 Elsevier

W is very small and only 4.5 μm, and at the same time, the density of SPSed W is only ~ 97%, due to its porosity in the matrix. That is to say, there are still favorable spaces for the growth of grains. For the hot-rolled ones, the relatively density is almost 100%, indicating that there is no direct growth space between grains. In addition, the cited pure W was rolled under a relatively high temperature (1500–1600 °C), resulting in a low density of dislocation defects because of the dynamic recrystallization during the hot-rolling process. Thus, the re-nucleation and grain growth of grains starting from dislocations were also limited. Therefore, the RCT of rolled W is higher than that of the SPSed one.

As described above, the nanoparticles added into the W matrix can pin GB and increase thermal activation energy of the grain migration and, therefore, enhance RCT. Xie et al. [29] fabricated W–0.5 wt% Y_2O_3 (WY05) and W–1.0 wt% Y_2O_3 (WY10) using the same technology as SPSed pure W. The metallographic analysis shows spherical tungsten grains in SPSed WY05 and SPSed WY10 with an average diameter of 4.0 and 3.2 μm, respectively, as shown in Fig. 4 [29]. The addition of 1.0 wt% Y_2O_3 could effectively prevent the growth of tungsten grains (4.1 μm in SPSed W), while it did not work with the addition of less than 0.5 wt% Y_2O_3, implying that a suitable amount of second-phase particles was important. Therefore, on the basis of SPSed results, WY10 was fabricated using hot-swaging deformation, because the deformation can further improve its mechanical properties [29, 33]. In the swaged WY10 sample, W grains are the round–bar shape with an average diameter and length of 4.6 and 26.7 μm, respectively, in swaged WY10, corresponding to an aspect ratio of 6:1. After annealing at 1300 °C for 1 h,

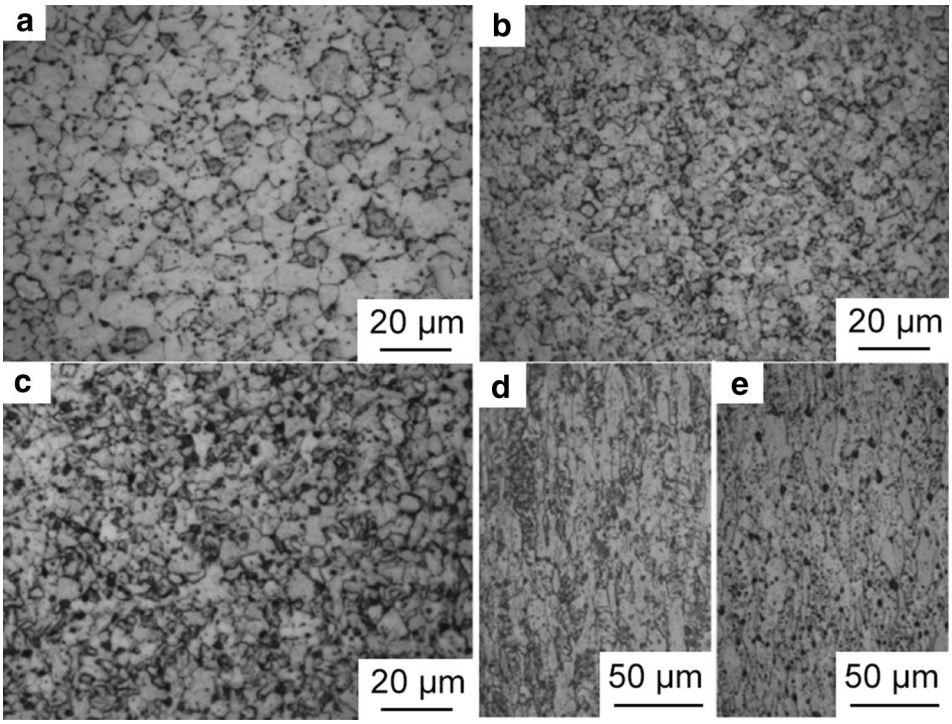

Fig. 4 Optical micrographs of **a** SPSed WY05, **b** SPSed WY10, **c** *R* plane of swaged WY10, **d** *L* plane of swaged WY10, and **e** *L* plane of annealed WY10. Reproduced with permission from Ref. [29]. Copyright 2015 Elsevier

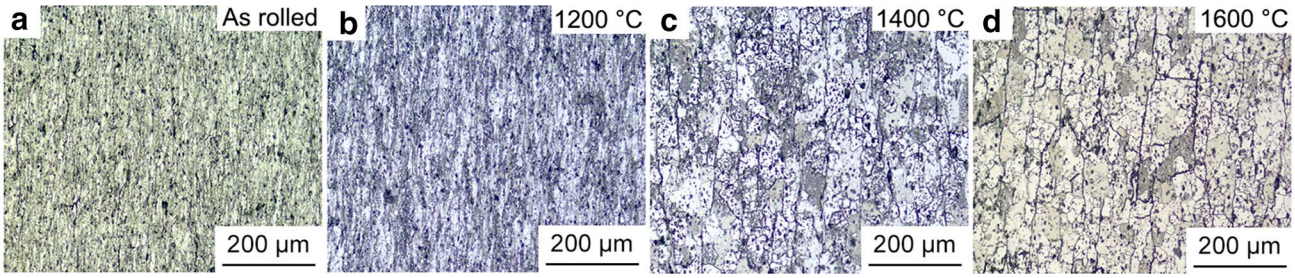

Fig. 5 Optical micrographs of as rolled and annealed WY10

the grain shape and size almost did not change, as shown in Fig. 4, indicating that swaged WY10 was thermostable with RCT higher than 1300 °C, which is higher than that of rolled pure W [19]. This is ascribed to the Y_2O_3 nanoparticle-pinning GBs, which restricts the migration of GBs and enhances the activation energy of the migration of GBs [29]. On the basis of swaged WY10, the thermal stability of hot-rolled WY10 fabricated by the same technology as that of hot-rolled pure W was investigated. The optical micrographs of the as-rolled and annealed WY10 indicate that the grain size of the specimen annealing at 1200 °C keeps the same as that of the as-rolled one (Fig. 5). However, after annealing at 1400 °C, the grain size increases obviously, implying that RCT of the rolled WY10 is between 1200 and 1400 °C (there is no data related to 1300 °C), which is similar to that of swaged WY10 [29], but higher than that of rolled pure W [19]. The nanosized K bubbles also can act as a dispersion-strengthening phase such as oxide particles. Tsuchida et al. [36] reported that the K-doped W with the bubble size of ~ 23–30 nm had RCT of ~ 1300 °C (Fig. 6 left), which was almost the same as that of rolled and swaged WY10 [38]. However, K-doped W–3 wt% Re has a higher RCT of 1400 °C (Fig. 6, right), which is 100 °C higher than those of W–K and WY10 [29, 36]. First, K bubbles and Y_2O_3 nanoparticles pinned the dislocations/dislocation networks and inhibited the migration of GBs [39], which leads to the higher RCT as compared with pure W. Furthermore, in K-doped W–Re alloy, solid solution Re atoms retard the nucleation of W grains and hinder the recrystallization by inhibiting the diffusion of W at high temperatures, resulting in a further increase of RCT [36].

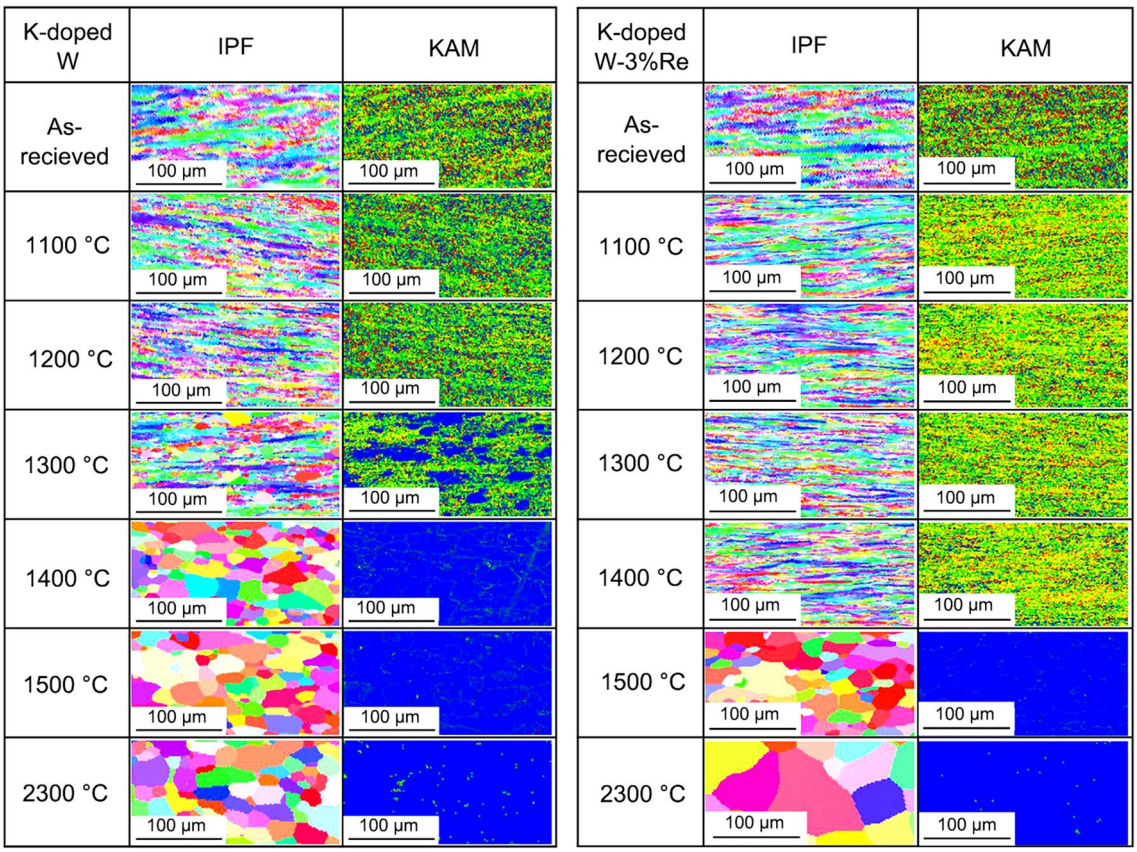

Fig. 6 Changes of the grain structure in K-doped W (left) and K-doped W–3 wt% Re by isochronous annealing for 1 h. Reproduced with permission from Ref. [36]. Copyright 2018 Elsevier

3 Thermal stability of carbide dispersion-strengthened tungsten alloys

As compared with the oxide-strengthened phases (e.g., Y_2O_3 ~ 2439 °C), the carbides such as TiC (~ 3140 °C), ZrC (~ 3530 °C), TaC (~ 3768 °C), and HfC (~ 3900 °C) have much higher melting temperatures which may result in higher thermal stabilities of the CDS-W compared with that of ODS-W. Miao et al. [40] prepared the W–0.5 wt% TiC plate by sintering in hydrogen, followed by hot rolling (the technology was the same as that of the rolled WY10 plate). Optical metallographic micrographs show the elongated grains in the as-rolled W–0.5 wt% TiC (Fig. 7a). After annealing at 1400 °C, the shape of grains keeps unchanged, as shown in Fig. 7b. After 1500 °C of annealing for 1 h, some grains become equiaxed, indicating the occurrence of recrystallization (Fig. 7c). With the annealing temperature further increasing to 1600 °C, grains grow apparently because of the full recrystallization, exhibiting a 100% size increase in the rolling direction (RD, an average length of 52.6 μm) and ~ 520% increase in transverse direction (TD, an average width of 47.7 μm), as presented in Fig. 7d. Therefore, the RCT of rolled W–0.5 wt% TiC is about 1400 °C [40], which is higher than those of WY10 and K-doped W. Liu et al. [41] prepared W–0.1%TiC using vacuum hot pressure and characterized the recrystallizaiton behaviour by investigating the evolutions of surface hardness and the grain size with annealing temperatures, and the RCT of W–0.1%TiC is ~ 1500 °C [41]. Xie et al. [23] developed ZrC nanoparticle dispersion-strengthened bulk W–0.5 wt% ZrC (WZC05) alloy by hot rolling. The thermal stability of this bulk WZC05 was investigated by isochronal experiments from 1000 to 1800 °C. The metallographic images of RD-normal direction (ND) planes of annealed specimens are presented in Fig. 8 [23]. Obviously, there are two different tungsten grains presented in the metallographic graphs: one is the fine elongated grain (Fig. 8a) with grey colour and another is the large equiaxed grain with bright appearance. Almost all grains keep the elongated form as the annealing temperature is below 1300 °C. With further increasing the annealing temperature to 1400 °C, a small fraction of equiaxed grains appear, and the aspect ratio of these elongated grains decreases significantly. Therefore, the RCT of the rolled WZC05 is between 1300 and 1400 °C.

For the rolled W–0.5 wt% TaC [42], the elongated grains have an average length of 41.7 μm along RD and a

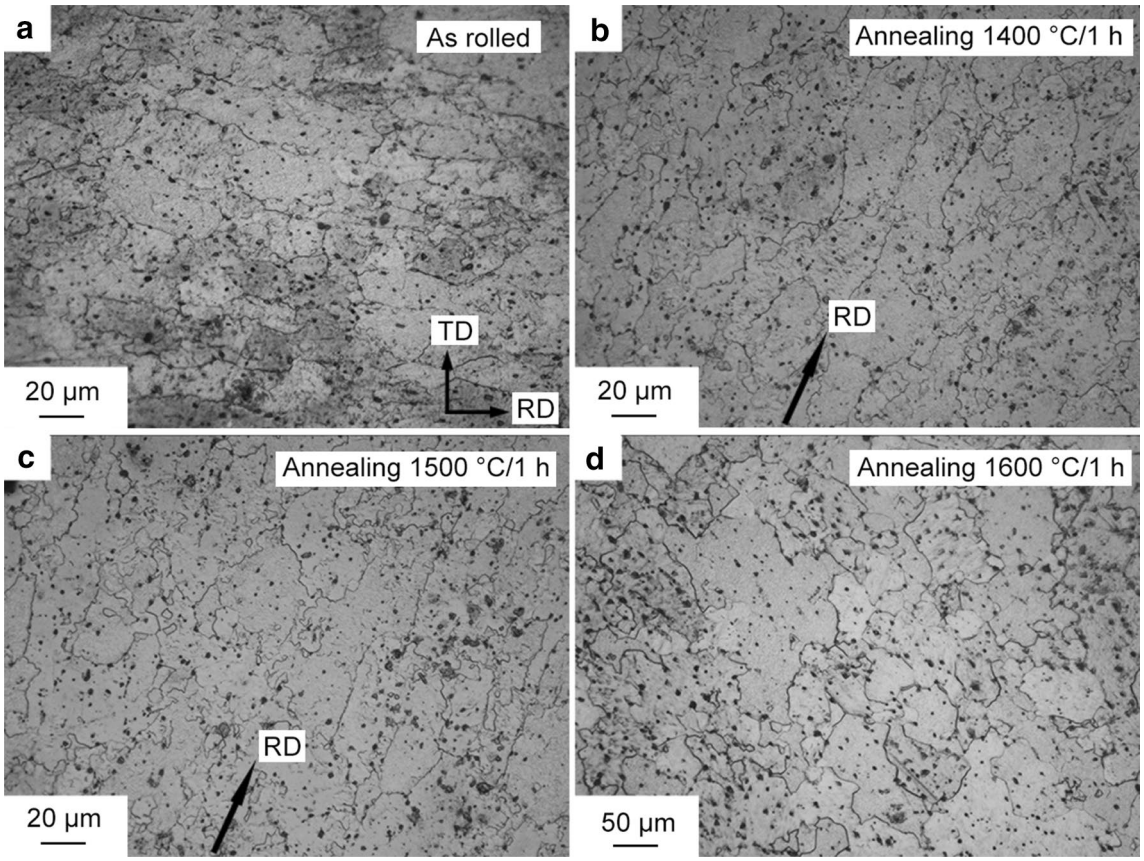

Fig. 7 Optical micrographs of **a** as-rolled W–0.5 wt% TiC alloy, **b–d** annealed W–0.5 wt% TiC alloy at 1400 °C, 1500 °C and 1600 °C, respectively. Reproduced with permission from Ref. [40]. Copyright 2016 Elsevier

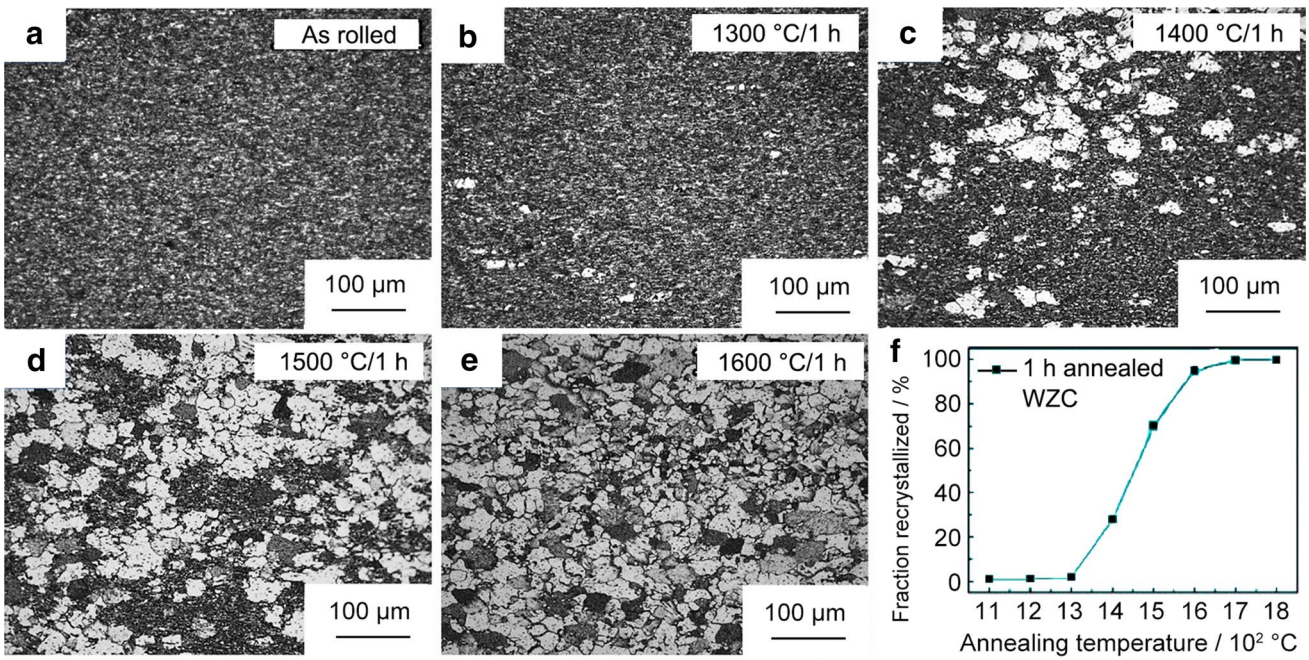

Fig. 8 Optical micrographs of **a** as-rolled W–0.5 wt% ZrC alloy, **b–e** annealed W–0.5 wt% ZrC alloy at 1300 °C, 1400 °C, 1500 °C and 1600 °C, respectively; **f** recrystallization fraction versus annealing temperature after treatments for 1 h. Reproduced with permission from Ref. [23]. Copyright 2017 Elsevier

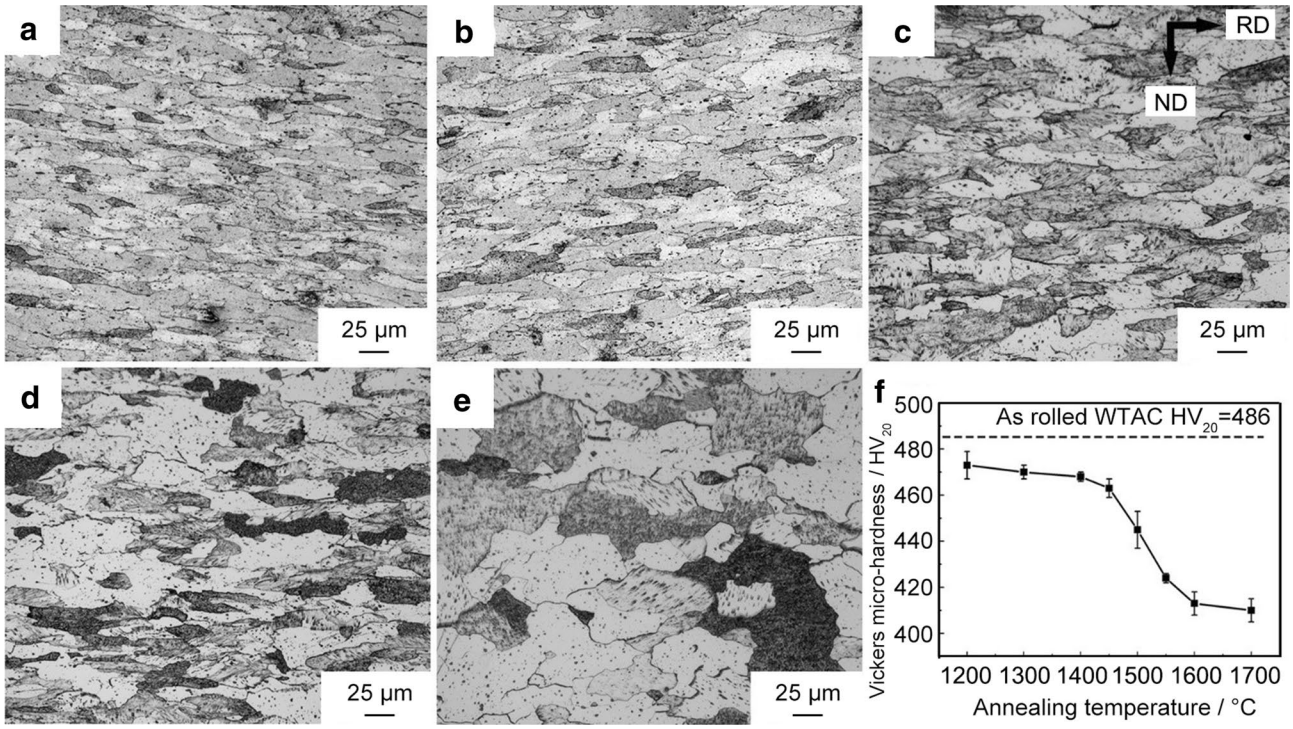

Fig. 9 Optical micrographs and Vickers hardness of W–0.5 wt% TaC annealing at various temperatures: **a** as-rolled samples, **b** 1400 °C, **c** 1450 °C, **d** 1500 °C, **e** 1600 °C, and **f** evolution of Vickers hardness with annealing temperature. Reproduced with permission from Ref. [42]. Copyright 2018 Elsevier

length–width ratio of 4:1. These grains keep stable until the annealing temperature reaching up to 1450 °C (Fig. 9a–c). After 1500 °C of annealing for 1 h, some grains grow up and become equiaxed, implying the occurrence of recrystallization (Fig. 9d). Further increasing the annealing temperature to 1600 °C, most grains recrystallize with a 210% of size increase in RD (an average length of 132.6 μm) and ~ 820% of size increase along ND (an average width of 83.2 μm), as shown in Fig. 9e. The RCT of the rolled W–0.5 wt% TaC is regarded as 1450 °C.

The rolled W–0.5 wt% HfC prepared by the same technology as that of rolled W–ZrC/TiC has elongated grains with an average length of 144.6 μm along RD and a width of 20 μm along ND, respectively, corresponding to a length–width ratio of 7.2:1 (Fig. 10a) [43]. Almost all grains kept the elongated form and the initial size until the annealing temperature reaches up to 1300 °C (Fig. 10b). When the temperature is up to 1400 °C, tungsten grains exhibit a slightly modified elongated form and the length–width ratio decreases to ~ 6.5:1 (Fig. 10c). For the specimen annealed at 1500 °C, some grains grow up, forming near-equiaxed structures (Fig. 10d). More than one-half of near-equiaxed grains appear after annealing at 1600 °C for 1 h (Fig. 10e). Especially, after annealing at 1800 °C, all the elongated tungsten grains are substituted by large equiaxed grains, as shown in Fig. 10f. Therefore, it could be concluded that RCT of the rolled W–0.5 wt% HfC is between 1400 and 1500 °C, and the full recrystallization temperature is ~ 1800 °C, which is 200 °C higher than that of rolled W–ZrC and W–TaC [17, 23].

As mentioned above, the solid solution Re atoms can suppress the recrystallization of W. Yang et al. [44] prepared W–1.0 wt% Re–0.5 wt% ZrC alloy by SPS sintering, and investigated its thermal stability by annealing for 2 h from 1300 to 1900 °C. Before annealing, the average size of the tungsten grain is ~ 2.6 μm. After annealing at 1300 °C, 1500 °C, 1700 °C, 1800 °C, and 1900 °C for 2 h, the average grain size increases to 2.7, 2.8, 2.8, 3.6, and 4.5 μm, respectively. Figure 11a indicates that the grain sizes of W keep unchanged when the annealing temperature is below 1800 °C, while the grain size significantly increases during 1800 °C annealing. Therefore, the RCT of W–1.0 wt% Re–0.5 wt% ZrC (W–ZrC–Re) is ~ 1700 °C, which is much higher than that of W–0.5 wt% ZrC. It is obvious that the addition of trace Re could significantly improve the thermal stability of W. Guo et al. [45] found that appropriate He bubbles induced by irradiation can not only strengthen W, but also retard the recrystallization of W.

As the hardness is very closely related to the grain size of materials, RCTs of different oxide/carbide dispersion-strengthened tungsten materials were summarized, by analyzing the evolution of Vickers micro-hardness

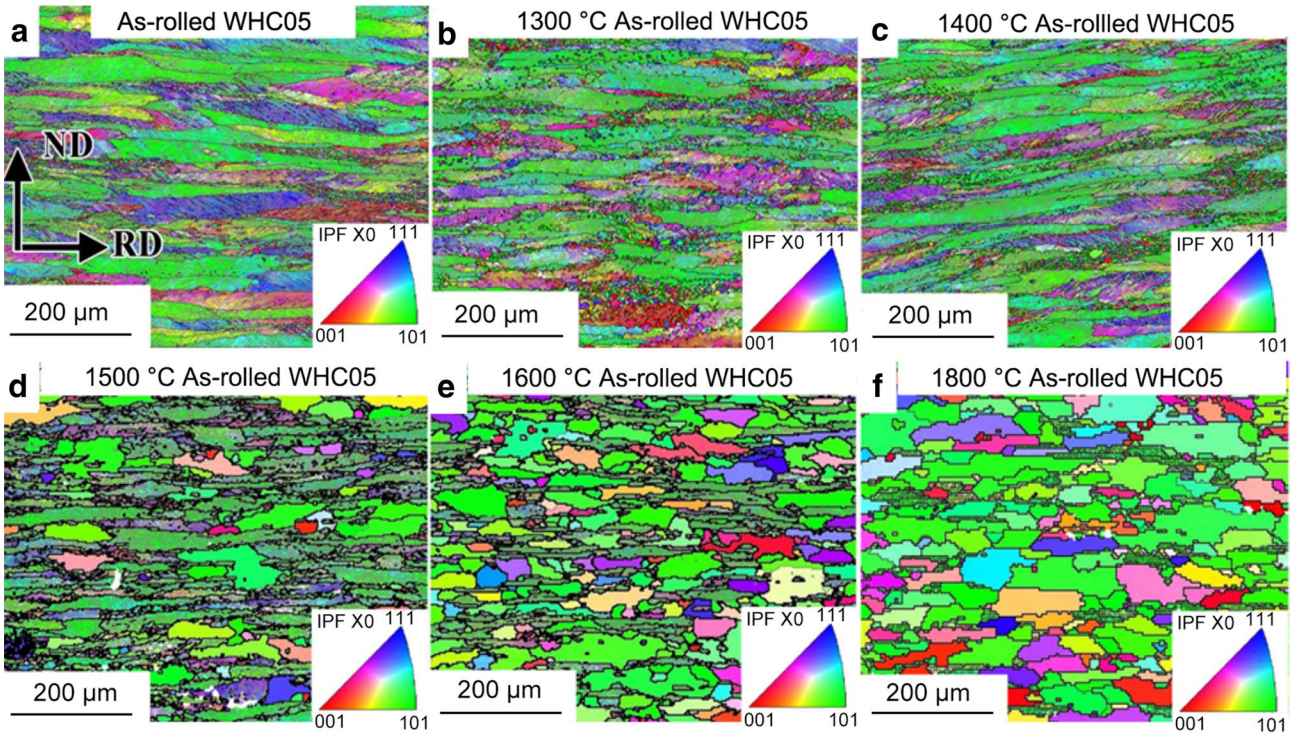

Fig. 10 Electron backscattered diffraction characterization of **a** as rolled, **b**–**e** W–0.5 wt% HfC alloys annealed at 1300 °C, 1400 °C, 1500 °C and 1600 °C, respectively, and **f** W–0.5 wt% HfC alloy annealed at 1800 °C. Reproduced with permission from Ref. [43]. Copyright 2019 Elsevier

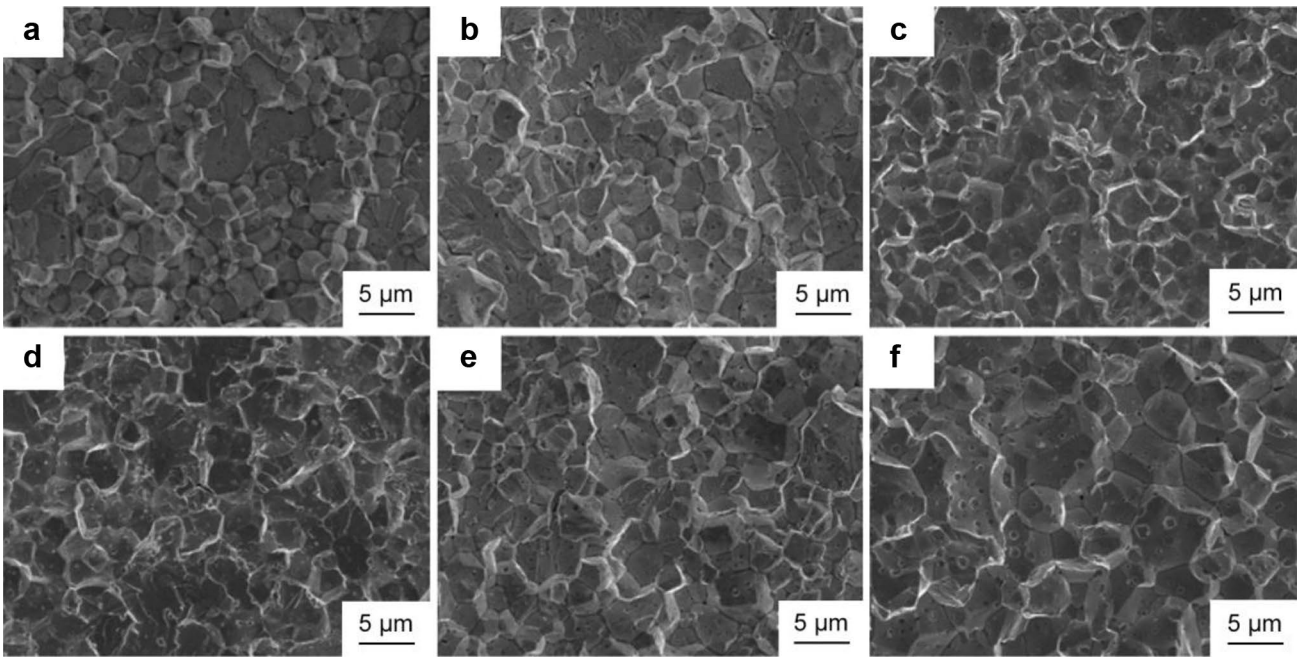

Fig. 11 SEM images of fracture surfaces of the W–ZrC–Re samples: **a** un-annealed, annealed at **b** 1300 °C, **c** 1500 °C, **d** 1700 °C, **e** 1800 °C, and **f** 1900 °C, respectively. Reproduced with permission from Ref. [44]. Copyright 2016 Elsevier

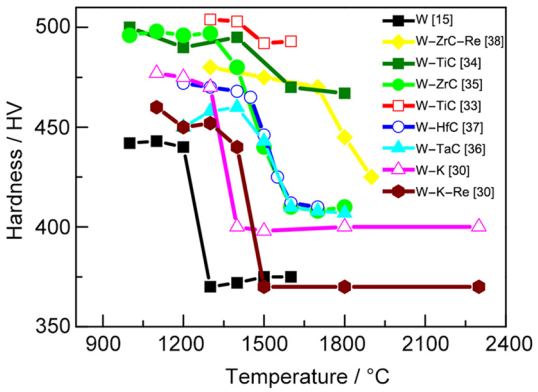

Fig. 12 Evolution of Vickers micro-hardness with annealing temperatures for different W materials

with annealing temperatures (Fig. 12). It is clear that the RCT of rolled pure W is the lowest (~ 1200 °C), and the second phase can significantly increase RCT: (1) for K-doped W, the RCT is ~ 1300 °C, (2) for ZrC, TiC, TaC, and HfC-doped W, RCTs are almost the same (~ 1400 °C) within experiment errors. The synergistic effect of different strengthening phases is prominent. For example, W–K–TiC alloys have the RCT of 1400–1600 °C with the contents of TiC from 0.05 to 1 wt% [46]. For K-doped W–3 wt% Re alloy, the RCT increases from 1300 to 1400 °C [35]. Moreover, for ZrC-doped W–Re alloy, the RCT is as high as 1700 °C [44]. It can be concluded that there is no obvious influence of the category of the second-phase particles on thermal stabilities of tungsten-based materials. For example, although TiC, ZrC, TaC, and HfC have different melt temperatures, the corresponding CDS-W materials possess almost the same RCTs within experiment errors. It is worth pointing out that the RCT of W–K wires can be as high as 1900 °C despite deformed by large plastic deformation such as cold drawing [47]. The possible reasons for such a high RCT may be ascribed to the following two aspects: (1) the fibrous grains elongate along the axial direction to form the so called Van Gogh sky structures and develop a very pronounced < 110 > fiber texture [48]; (2) individual well-shaped and spherical nano-K bubble rows formed during heating wires to higher temperatures could inhibit motion of most longitudinal grain boundaries and hinder triple junction motion, resulting in highly stable fiber structures [49].

4 Conclusion and outlook

The thermal stability is very important for tungsten-based materials as PFCs, which determines the servicing performance at high temperatures. RCT, as a parameter to characterize the thermal stability of materials, is determined by the evolutions of grain sizes and Vickers hardness with annealing temperatures. This paper reviews the effects of different dispersion-strengthening phases on the RCT of W materials. The second-phase particles could pin the GB and hinder its migration, which significantly raise RCTs of W materials. For different kinds of particles such as oxides, K bubbles, and carbides, there is no obvious influence of the category of the second-phase particles on thermal stabilities of tungsten-based materials. On the other hand, RCT may depend on the original microstructure much. The particle size and the number density of strengthening particles could influence the RCT, because the higher the number density of finer particles is, the stronger the pinning ability is, which leads to a higher RCT. Therefore, for certain dispersion-strengthening W materials, refining-strengthening particles could further improve the RCT, because for the same content of the second-phase particles, the smaller the size is, the larger the number density is, resulting in stronger pinning effects on migration of grain boundaries. Meanwhile, the fabrication technology pronouncedly influences on the RCT by changing the microstructures. For example, the hot-rolled W has a higher RCT than that of SPSed W. Moreover, the different deformation degrees can produce different textures, for example, the different proportion of high angle grain boundary and low angle grain boundary, and distributions of the second-phase particles, which should have a significant effect on RCT. However, there are no specific data about the effect of deformation degrees on RCT. In this work, the hot-rolled W–ZrC/HfC/TaC/TiC plates have the same deformation degree: reduction of ~ 70%, but the deformation degrees of W–K and W–K–Re plates are unknown. Therefore, optimizing the technology can further improve the thermal stability of tungsten materials.

Acknowledgements This work was financially supported by the National Natural Science Foundation of China (Grant Nos. 51771184, 11735015, 11575241, 51801203 and 11575231), the Natural Science Foundation of Anhui Province (Grant No. 1808085QE132) and the Open Project of State Key Laboratory of Environment Friendly Energy Materials(Grant No. 18kfhg02).

References

1. Norajitra P, Boccaccini LV, Gervash A, Giniyatulin R, Holstein N, Ihli T, Janeschitz G, Krauss W, Kruessmann R, Kuznetsov V, Makhankov A, Mazul I, Moeslang A, Ovchinnikov I, Rieth M, Zeep B. Development of a helium-cooled divertor: material choice and technological studies. J Nucl Mater. 2007;367–370:1416.
2. Philipps V. Tungsten as material for plasma-facing components in fusion devices. J Nucl Mater. 2011;415(1):S2.
3. Neu R, Dux R, Kallenbach A, Putterich T, Balden M, Fuchs JC, Herrmann A, Maggi CF, O'Mullane M, Pugno R, Radivojevic I, Rohde V, Sips ACC, Suttrop W, Whiteford A, The ASDEX

Upgrade Team. Tungsten: an option for divertor and main chamber plasma facing components in future fusion devices. Nucl Fusion. 2005;45(3):209.
4. Rupp D, Mönig R, Gruber PA, Weygand SM. Fracture toughness and microstructural characterization of polycrystalline rolled tungsten. Int J Refract Met Hard Mater. 2010;28(6):669.
5. Wurster S, Gludovatz B, Hoffmann A, Pippan R. Fracture behaviour of tungsten–vanadium and tungsten–tantalum alloys and composites. J Nucl Mater. 2011;413(3):166.
6. Xia M, Yan Q, Xu L, Guo H, Zhu L, Ge C. Bulk tungsten with uniformly dispersed La_2O_3 nanoparticles sintered from co-precipitated La_2O_3/W nanoparticles. J Nucl Mater. 2013;434(1–3):85.
7. Ueda Y, Schmid K, Balden M, Coenen JW, Loewenhoff TH, Ito A, Hasegawa A, Hardie C, Porton M, Gilbert MR. Baseline high heat flux and plasma facing materials for fusion. Nucl Fusion. 2017;57(9):092006.
8. El-Guebaly L, Kurtz R, Rieth M, Kurishita H, Robinson A, ARIES Team. W-based alloys for advanced divertor designs: options and environmental impact of state-of-the-art alloys. Fusion Sci Technol. 2011;60(1):185.
9. Miki N, Verrecchia M, Barabaschi P, Belov A, Chiocchio S, Elio F, Ioki K, Kikuchi S, Kokotkov V, Ohmori J, Roccella M, Sonato P, Testoni P, Utin Y. Vertical displacement event/disruption electromagnetic analysis for the ITER-FEAT vacuum vessel and in-vessel components. Fusion Eng Des. 2001;58–59:555.
10. Abdullaev SS, Finken KH, Wongrach K, Tokar M, Koslowski HR, Willi O, Zeng L. Mechanisms of plasma disruption and runaway electron losses in the TEXTOR tokmak. J Plasma Phys. 2015;81(5):475810501.
11. Bolt H, Barabash V, Federici G, Linke J, Loarte A, Roth J, Sato K. Plasma facing and high heat flux materials–needs for ITER and beyond. J Nucl Mater. 2002;307–311(Part 1):43.
12. Maddaluno G, Maruccia G, Merola M, Rollet S. Energy deposition and thermal effects of runaway electrons in ITER-FEAT plasma facing components. J Nucl Mater. 2003;313–316:651.
13. Romaner L, Ambrosch-Draxl C, Pippan R. Effect of rhenium on the dislocation core structure in tungsten. Phys Rev Lett. 2010;104(19):195503.
14. Kurishita H, Arakawa H, Matsuo S, Sakamoto T, Kobayashi S, Nakai K, Pintsuk G, Linke J, Tsurekawa S, Yardley V, Tokunaga K, Takida T, Katoh M, Ikegaya A, Ueda Y, Kawai M, Yoshida N. Development of nanostructured tungsten based materials resistant to recrystallization and/or radiation induced embrittlement. Mater Trans. 2013;54(4):456.
15. Rieth M, Dudarev SL, de Vicente GSM, Aktaa J, Ahlgren T, Antusch S, Armstrong DEJ, Balden M, Baluc N, Barthe MF, Basuki WW, Battabyal M, Becquart CS, Blagoeva D, Boldyryeva H, Brinkmann J, Celino M, Ciupinski L, Correia JB, De Backer A, Domain C, Gaganidze E, García-Rosales C, Gibson J, Gilbert MR, Giusepponi S, Gludovatz B, Greuner H, Heinola K, Höschen T, Hoffmann A, Holstein N, Koch F, Krauss W, Li H, Lindig S, Linke J, Linsmeier CH, López-Ruiz P, Maier H, Matejicek J, Mishra TP, Muhammed M, Muñoz A, Muzyk M, Nordlund K, Nguyen-Manh D, Opschoor J, Ordás N, Palacios T, Pintsuk G, Pippan R, Reiser J, Riesch J, Roberts SG, Romaner L, Rosiński M, Sanchez M, Schulmeyer W, Traxler H, Ureña A, van der Laan JG, Veleva L, Wahlberg S, Walter M, Weber T, Weitkamp T, Wurster S, Yar MA, You JH, Zivelonghi A. Recent progress in research on tungsten materials for nuclear fusion applications in Europe. J Nucl Mater. 2013;432(1–3):482.
16. Huang B, Tang J, Chen L, Yang X, Lian Y, Chen L, Liu X, Cui X, Gu L, Liu CT. Design of highly thermal-shock resistant tungsten alloys with nanoscaled intra- and inter-type K bubbles. J Alloy Compd. 2019;782:149.
17. Liu R, Xie ZM, Hao T, Zhou Y, Wang XP, Fang QF, Liu CS. Fabricating high performance tungsten alloys through zirconium micro-alloying and nano-sized yttria dispersion strengthening. J Nucl Mater. 2014;451(1–3):35.
18. Wu Y. Manufacturing of tungsten and tungsten composites for fusion application via different routes. Tungsten. 2019;1:80.
19. Deng H, Xie Z, Wang YK, Liu R, Zhang T, Hao T, Wang XP, Fang QF, Liu CS. Mechanical properties and thermal stability of pure W and W–0.5 wt% ZrC alloy manufactured with the same technology. Mater Sci Eng A. 2018;715:117.
20. Kurishita H, Matsuo S, Arakawa H, Sakamoto T, Kobayashi S, Nakai K, Takida T, Kato M, Kawai M, Yoshida N. Development of re-crystallized W–1.1% TiC with enhanced room-temperature ductility and radiation performance. J Nucl Mater. 2010;398(1–3):87.
21. Zhang T, Yan W, Xie Z, Miao S, Yang J, Wang X, Fang Q, Liu C. Recent progress of oxide/carbide dispersion strengthened W-based materials. Acta Metall Sin. 2018;54:831.
22. Wang YK, Miao S, Xie ZM, Liu R, Zhang T, Fang QF, Hao T, Wang XP, Liu CS, Liu X, Cai LH. Thermal stability and mechanical properties of HfC dispersion strengthened W alloys as plasma-facing components in fusion devices. J Nucl Mater. 2017;492:260.
23. Xie ZM, Miao S, Liu R, Zeng LF, Zhang T, Fang QF, Liu CS, Wang XP, Lian YY, Liu X, Cai LH. Recrystallization and thermal shock fatigue resistance of nanoscale ZrC dispersion strengthened W alloys as plasma-facing components in fusion devices. J Nucl Mater. 2017;496:41.
24. Dong Z, Liu N, Ma Z, Liu C, Guo Q, Yamauchi Y, Alamri HR, Alothman ZA, Hossain MSA, Liu Y. Synthesis of nanosized composite powders via a wet chemical process for sintering high performance W–Y_2O_3 alloy. Int J Refract Met Hard Mater. 2017;69:266.
25. Fan J, Han Y, Li P, Sun Z, Zhou Q. Micro/nano composited tungsten materials and its high thermal loading behavior. J Nucl Mater. 2014;455(1–3):717.
26. Lian Y, Liu X, Feng F, Song J, Yan B, Wang Y, Wang J, Chen Z. Mechanical properties and thermal shock performance of W–Y_2O_3 composite prepared by high-energy-rate forging. Phys Scr. 2017;T170:014044.
27. Battabyal M, Schäublin R, Spätig P, Baluc N. W–2 wt% Y_2O_3 composite: microstructure and mechanical properties. Mater Sci Eng A. 2012;538:53.
28. Zhang J, Ma S, Zhu J, Kang K, Luo G, Wu C, Shen Q, Zhang L. Microstructure and compression strength of W/HfC composites synthesized by plasma activated sintering. Met Mater Int. 2019;25:416.
29. Xie ZM, Liu R, Miao S, Zhang T, Wang XP, Fang QF, Liu CS, Luo GN. Effect of high temperature swaging and annealing on the mechanical properties and thermal conductivity of W–Y2O3. J Nucl Mater. 2015;464:193.
30. Zhao M, Zhou Z, Zhong M, Tan J. Effect of hot rolling on the microstructure and fracture behavior of a bulk fine-grained W–Y2O3 alloy. Mater Sci Eng A. 2015;646:19.
31. Luo LM, Tan XY, Chen HY, Luo GN, Zhu XY, Cheng JG, Wu YC. Preparation and characteristics of W–1 wt% TiC alloy via a novel chemical method and spark plasma sintering. Powder Technol. 2015;273:8.
32. Feng F, Lian Y, Liu X, Wang J, Xu Y. Effect of high-energy-rate forging on microstructure and properties of W–TaC alloys. IEEE Trans Plasma Sci. 2017;46:2314.
33. Kang K, Zhang L, Luo G, Zhang J, Tu R, Wu C, Shen Q. Microstructural evolution and mechanical behavior of W–Si–C multiphase composite prepared by arc-melting. Mater Sci Eng A. 2018;712:28.
34. Xie ZM, Zhang T, Liu R, Fang QF, Miao S, Wang XP, Liu CS. Grain growth behavior and mechanical properties of zirconium micro-alloyed and nano-size zirconium carbide dispersion

strengthened tungsten alloys. Int J Refract Met Hard Mater. 2015;51:180.
35. Liu R, Xie ZM, Yang JF, Zhang T, Hao T, Wang XP, Fang QF, Liu CS. Recent progress on the R&D of W–ZrC alloys for plasma facing components in fusion devices. Nucl Mater Energy. 2018;16:191.
36. Tsuchida K, Miyazawa T, Hasegawa A, Nogami S, Fukuda M. Recrystallization behavior of hot-rolled pure tungsten and its alloy plates during high-temperature annealing. Nucl Mater Energy. 2018;15:158.
37. Ren C, Fang Z, Xu L, Ligda JP, Paramore JD, Butler BG. An investigation of the microstructure and ductility of annealed cold-rolled tungsten. Acta Mater. 2019;162:202.
38. Xie ZM, Liu R, Zhang T, Fang QF, Liu CS, Liu X, Luo GN. Achieving high strength/ductility in bulk W–Zr–Y_2O_3 alloy plate with hybrid microstructure. Mater Des. 2016;107:144.
39. Zan X, Gu M, Wang K, Luo L, Zhu X, Wu Y. Recrystallization kinetics of 50% hot-rolled 2% Y_2O_3 dispersed tungsten. Fusion Eng Des. 2019;144:1.
40. Miao S, Xie ZM, Zhang T, Wang XP, Fang QF, Liu CS, Luo GN, Liu X, Lian YY. Mechanical properties and thermal stability of rolled W–0.5 wt% TiC alloys. Mater Sci Eng A. 2016;671:87.
41. Liu X, Chen J, Lian Y, Wu J, Xu Z, Zhang N, Wang Q, Duan X, Wang Z, Zhong J. Vacuum hot-pressed beryllium and TiC dispersion strengthened tungsten alloy developments for ITER and future fusion reactors. J Nucl Mater. 2013;442(1–3):S309.
42. Xie ZM, Miao S, Zhang T, Liu R, Wang XP, Fang QF, Hao T, Zhuang Z, Liu CS, Lian YY, Liu X, Cai LH. Recrystallization behavior and thermal shock resistance of the W–1.0 wt% TaC alloy. J Nucl Mater. 2018;501:282.
43. Wang YK, Xie ZM, Wang MM, Deng HW, Yang JF, Jiang Y, Zhang T, Wang XP, Fang QF, Liu CS. The superior thermal stability and tensile properties of hot rolled W–HfC alloys. J Refract Metals Hard Mater. 2019;81:42.
44. Yang XD, Xie ZM, Miao S, Liu R, Jiang WB, Zhang T, Wang XP, Fang QF, Liu CS, Luo GN, Liu X. Tungsten-zirconium carbide-rhenium alloys with extraordinary thermal stability. Fusion Eng Des. 2016;106:56.
45. Guo W, Cheng L, De Temmerman G, Yuan Y, Lu GH. Retarded recrystallization of helium-exposed tungsten. Nucl Fusion. 2018;58:106011.
46. Shi K, Huang B, He B, Xiao Y, Chen L, Lian Y, Liu X, Tang J. Recrystallization behavior after annealing and thermal shock tests of W–K–TiC alloy. Fusion Eng Des. 2017;122:223.
47. Briant CL, Horacsek O, Horacsek K. The effect of wire history on the coarsened substructure and secondary recrystallization of doped tungsten. Metall Trans A. 1993;24(4):843.
48. Nikolić V, Riesch J, Pippan R. The effect of heat treatments on pure and potassium doped drawn tungsten wires: part I-microstructural characterization. Mater Sci Eng A. 2018;737:422.
49. Schade P. Potassium bubble growth in doped tungsten. Int J Refract Met Hard Mater. 1998;16(1):77.

Professor Tao Zhang is a full professor of Materials Science in Guangzhou University. He received his Ph.D. degree from University of Sciences and Technology of China in 2007. Then he worked as Humboldt Research Fellow at Stuttgart University, Germany, in 2008–2009 and Post Doctor in Paul Scherrer Institute, Switzerland, in 2011–2013, respectively. His research interests are key materials of nuclear energy and irradiation damage of materials and high entropy alloy. He has published over 100 peer-reviewed papers in Applied Physics Review, Acta Materialia, Materials & Design and so on.